applied sciences

MDPI

Article

Development of Nd-Doped $CaWO_4$ Single Crystalline Scintillators Emitting Near-Infrared Light

Kai Okazaki, Daisuke Nakauchi, Hiroyuki Fukushima, Takumi Kato, Noriaki Kawaguchi and Takayuki Yanagida *

Division of Materials Science, Nara Institute of Science and Technology (NAIST), 8916-5 Takayama-Cho, Ikoma City 630-0192, Nara, Japan
* Correspondence: t-yanagida@ms.naist.jp

Abstract: Nd-doped $CaWO_4$ single crystals with dopant concentrations of 0.1, 0.5, and 1% were synthesized by the floating zone method. The transmission, photoluminescence, and scintillation properties were evaluated from ultraviolet to near-infrared (NIR) ranges. An emission peak due to transitions of the host was observed at 400 nm, and several sharp peaks originating from Nd^{3+} 4f–4f transitions were confirmed at 900, 1060, and 1300 nm. The quantum yields of 0.1, 0.5, and 1% Nd-doped samples were 70.7, 79.5, and 61.2%, respectively, when monitored, and excited wavelengths were 750–1500 nm and 590 nm. Decay times consistent with typical Nd^{3+} transitions were obtained when NIR ranges were monitored. Additionally, the energy transfer between the host and Nd^{3+} occurred according to the decay measurement. The relationship between X-ray irradiated dose rate and intensity in the range of NIR was investigated by combining the crystals with an InGaAs-photodiode. The lowest detectable dose rate retaining the linearity of the present crystals was 0.3–0.06 Gy/h.

Keywords: scintillation; photoluminescence; 4f–4f transition; floating zone method

check for updates

Citation: Okazaki, K.; Nakauchi, D.; Fukushima, H.; Kato, T.; Kawaguchi, N.; Yanagida, T. Development of Nd-Doped $CaWO_4$ Single Crystalline Scintillators Emitting Near-Infrared Light. *Appl. Sci.* **2022**, *12*, 11624. https://doi.org/10.3390/app122211624

Academic Editor: Burkhard Poeggeler

Received: 8 October 2022
Accepted: 15 November 2022
Published: 16 November 2022

1. Introduction

Scintillators have a function to convert high-energy photons like X- and γ-rays into many low-energy photons after absorbing the energy immediately. They have been practically used for radiation detections combined with photodetectors [1]. The application fields are widespread: medical [2], security [3], space exploration [4], high-energy physics [5], and resource exploration [6]. Scintillators with ultraviolet (UV)–visible light emitting have been mainly studied [7–10] because conventional detectors like photomultiplier tubes (PMTs) have wavelength sensitivity at the corresponding regions [11,12]. However, photodetectors having wavelength sensitivity at NIR ranges have been proposed, such as PbS [13], InSb [14], and InGaAs-based detectors [15]. Hence, NIR photons became detected, and the development of scintillators emitting NIR light (NIR-scintillators) has attracted much attention [16].

NIR scintillators are especially considered to be used in biological imaging and high-dose field monitoring. They can realize the in vivo depth imaging [16] owing to the unique characteristics of NIR light, such as high transparency for human soft tissues [17]. Additionally, they have an advantage in high-dose monitoring inside and around nuclear reactors compared with scintillators emitting UV–visible light [18]. Bluish-white Cherenkov lights are usually generated in nuclear reactors, and the scintillation detector is used in this environment. When conventional scintillators with visible emission wavelength are used in this situation, true and background Cherenkov signals are difficult to distinguish. On the contrary, NIR light can be easily distinguished from them because the intensity of Cherenkov light is inverse proportion to $\sim\lambda^2$ [19]; hence, the signal-to-noise ratio of scintillation light at the NIR range would be increased. Furthermore, a remote dose monitoring system with optical fibers having resistance to radiation is suggested for monitoring the environment [20]. NIR light produces low transmission losses in quartz fibers, while the

degradation in the visible range is largely even in radiation-resistive optical fibers [21]. High interaction probabilities for X- and γ-rays and high radiation hardness are desired for scintillators to use in the above applications where the dose rate is very high. A $CaWO_4$ single crystal is a candidate for the host material. This material has a large effective atomic number (Z_{eff}, 62); thus, radiation detection efficiency can be improved as photoabsorption, Compton scattering, and pair creations are relatively proportional to ~Z_{eff}^4, ~Z_{eff}, and ~Z_{eff}^2 [22], respectively. Additionally, the transmittance of the material in NIR regions is reported to change little after high-dose irradiation [23], although the transmittance of UV-visible ranges degrades largely after a huge exposure. In terms of luminescence centers, some rare-earth ions have a function to show NIR luminescence [24]. Nd^{3+} has especially attracted interest as NIR luminescent centers. Typical main emissions of Nd^{3+} are confirmed at ~1060 nm, and the emission is applied in laser fields such as Nd: $Y_3Al_5O_{12}$ lasers [25]. Further, NIR-scintillation has been observed in some Nd-doped scintillators [26–28]. In the study, Nd-doped $CaWO_4$ single crystals were grown as NIR-scintillators, and we evaluated the optical and scintillation properties.

2. Materials and Methods

$CaWO_4$ single crystals doped with various concentrations of Nd (0.1, 0.5, and 1 at%) were grown with the floating zone (FZ) method. First, starting materials: CaO (Furuuchi Chemical, 99.99%), WO_2 (Rare Metallic, 99.9%), and Nd_2O_3 (Rare Metallic, 99.99%) were mixed and sintered at 600 °C for 8 h. After that, they molded into rod-shaped and sintered at 1200 °C for 8 h. And then, polycrystalline rods were obtained. By using the rods, we conducted the crystal growth with the FZ furnace (Canon Machinery, FZD0192) having dual Halogen lamps. The condition of the rotation rate and the pulling-down rate were 14 rpm and 5 mm/h. To confirm the crystalline phases of the present crystals, powder X-ray diffraction (XRD) measurements were conducted with a diffractometer (Rigaku, MiniFlex600).

The measurement of diffuse transmission spectra was performed with a spectrophotometer (Shimadzu, SolidSpec-3700) as a basic optical property. The tested ranges were 270–1600 nm. Both a PMT and an InGaAs-based detector were mounted in the spectrophotometer, and they respectively monitored at 270–870 nm and 870–1600 nm by different photodetectors. In the evaluation of photoluminescence (PL) properties, PL excitation and emission contour maps were measured with a Quantaurus-QY Plus (Hamamatsu, C11367). The excitation and monitored wavelengths were 250–850 nm and 195–1675 nm, respectively. PL decay curves were measured with a Quantaurus-τ (Hamamatsu, C13534).

As radiation-induced luminescence properties, X-ray-induced scintillation spectra, decay curves, afterglow curves, and dose rate response properties were evaluated by our original setups [29–31]. In the measurement of dose rate response properties, the NIR-scintillation light from the samples was detected by an InGaAs-photodiode (PD) (Hamamatsu, G12180-250A). The light was carried via a fiber (Thorlabs, FP600ERT) of 5 m in length and 600 μm φ, and it simulated actual applications. The signals from the PD were analyzed as currents using a picoammeter (Keysight, B2985A).

3. Results and Discussion

After the crystal growth, rods with ~20 mm length and ~5 mm φ were obtained. They were cut and polished for the evaluation of optical and scintillation characteristics. Figure 1 shows the appearance of the prepared crystals. The length and thickness were ~3 mm and ~1 mm. All the crystals were transparent, and appeared pale blue as the dopant concentration increased.

Some of the remained parts of as-grown rods after the single crystal growth were crushed, and the crashed powders were used for the XRD measurement. The obtained patterns and a reference from the Crystallography Open Database (COD: 9009627) are indicated in Figure 2. All the patterns matched that of the reference. Impurity phases such as CaO, WO_2, and WO_3 were not confirmed.

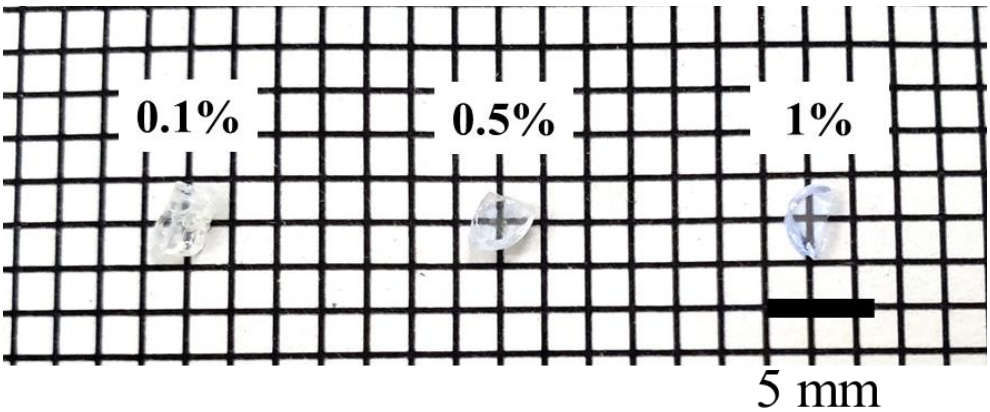

Figure 1. Photograph of Nd-doped $CaWO_4$.

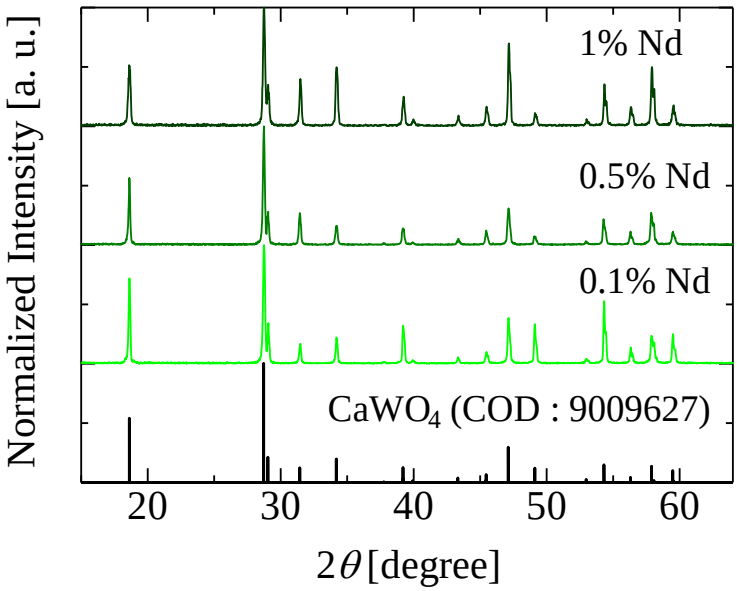

Figure 2. XRD patterns of Nd-doped $CaWO_4$ with reference.

The diffuse transmission spectra of the crystals are shown in Figure 3. The transmission spectra at 850–900 nm were not described because noise due to a detector switching from a PMT to an InGaAs-based detector was dominant in the range. The transmittance was ~70–90% in the range from 330 to 1600 nm, although signals at 900–1000 nm were especially unstable owing to noise from a detector switching. Absorption was observed at 270 nm, originating from the transition from the 2p states of O^{2-} to the 5d states of W^{6+} in $(WO_4)^{2-}$ [32,33]. Additionally, some absorption bands were confirmed at 350, 520, 590, 750, and 800 nm. They originated from the transitions from the $^4I_{9/2}$ level to the $^2I_{11/2}$, $^2G_{9/2}$, $^2G_{7/2}$, $^4S_{3/2}$, and $^4F_{5/2}$ levels of Nd^{3+} [34].

The excitation and emission contour maps of the 1% Nd-doped $CaWO_4$ crystal are exhibited in Figure 4a,b as a representative. No significant change was observed in the spectral shapes of the other two crystals. The vertical axis presents the excitation wavelength, and the horizontal axis presents the emission wavelength. A broad emission band was confirmed at 350–500 nm under excitation wavelength at 250–300 nm. It would be derived from the host ($CaWO_4$) [35]. In the NIR range, some emissions were confirmed at 900, 1060, and 1300 nm, and they were ascribed to the typical emissions derived from the 4f–4f transitions of Nd^{3+} [34,35]. The quantum yields (QY) of the crystals accumulated 750–1500 nm under excitation at 590 nm of 0.1, 0.5, and 1% doped samples were 70.7, 79.5, and 61.2%, respectively.

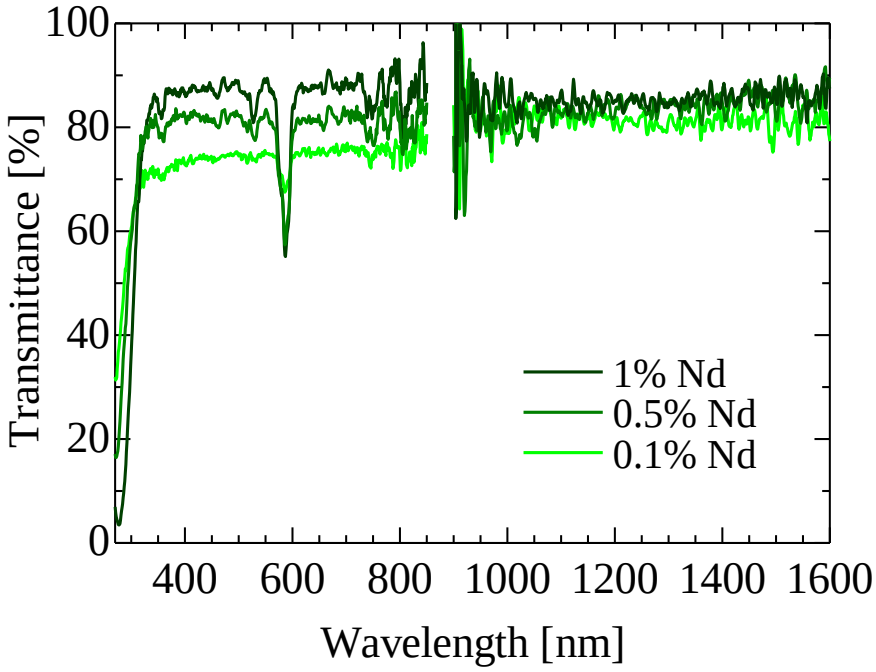

Figure 3. Diffuse transmission spectra of Nd-doped $CaWO_4$.

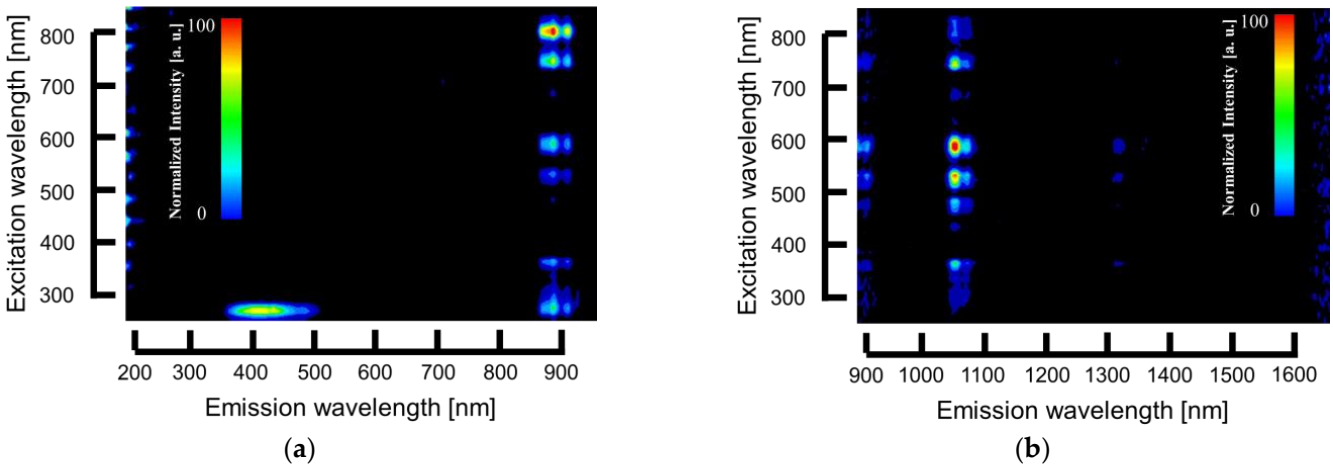

Figure 4. PL excitation and emission contour maps of 1% Nd-doped $CaWO_4$ monitored (**a**) 195–950 nm and (**b**) 895–1675 nm.

The PL decay curves were measured to confirm the origin of the emissions. Figure 5a exhibits the PL decay curves monitored at 420 nm. The excitation wavelength was selected to 280 nm. The decay curves were composed of the sum of two exponential functions. The fast components were attributed to the Instrumental response function (IRF) due to the excitation source. The slow components with decay times of ~7–9 µs would be derived from the charge transfer transition in $(WO_4)^{2-}$ anion complex [36]. The decay curves monitored at 880 nm are exhibited in Figure 5b. The excitation wavelength was set to 575–625 nm. The curves were agreed with an exponential function with decay times of ~160 µs. The decay times were consistent with the reasonable values as the $^4F_{3/2}$–$^4I_{9/2}$ transition of Nd^{3+} was reported in other phosphors doped with Nd [37,38].

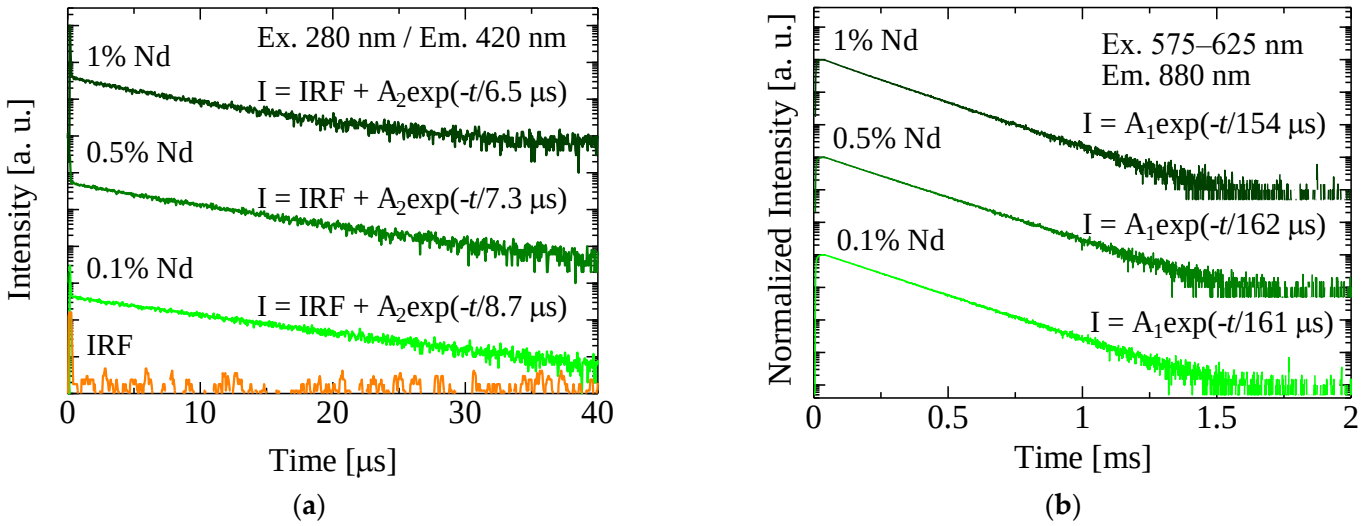

Figure 5. PL decay curves of Nd-doped $CaWO_4$ (**a**) monitored at 420 nm under excitation at 280 nm and (**b**) monitored at 880 nm under excitation at 575–625 nm.

Figure 6a,b show the X-ray-induced scintillation spectra of the crystals when monitored at 300–600 nm and 700–1500 nm, respectively. A broad emission with the peak top at 420 nm was observed at 300–600 nm. The emission is composed of double peaks derived from the charge transfer transition in $(WO_4)^{2-}$ anion complex and some defects such as oxygen and lattice defects [39]. In the NIR range, some sharp emission lines were confirmed at 900, 1060, and 1300 nm. Almost the same spectral features due to Nd^{3+} were observed in other materials doped with Nd [40–42]; hence the emissions would originate from the Nd^{3+}.

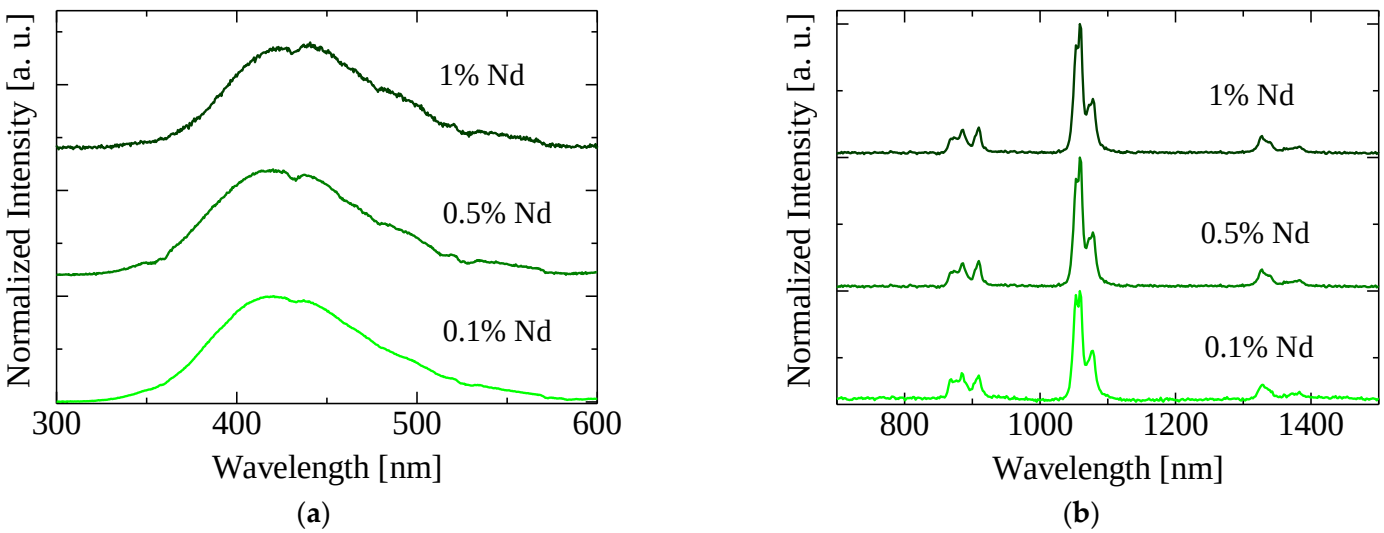

Figure 6. X-ray-induced scintillation spectra of Nd-doped $CaWO_4$ monitored (**a**) 300–600 nm and (**b**) 700–1500 nm.

The X-ray-induced scintillation decay curves monitored at the range from UV to visible light are exhibited in Figure 7a. They were well agreed with a sum of two exponential functions. The origin of the fast (~1 μs) and slow (~5–7 μs) components were respectively considered to be the WO_3–V_O complex defects and the charge transfer transitions in $(WO_4)^{2-}$ anion complex because the confirmed decay times were comparable with the scintillation decay times of $CaWO_4$, reported in the past study [43]. The slow components became fast as the Nd concentration increased. It presented that the energy transfer from the host to Nd^{3+} happened because the emission due to the host partially matched

with the excitation bands of Nd^{3+}, as shown in Figure 4. Figure 7b shows the decay curves monitored at visible–NIR ranges. The obtained curves were well-matched with two exponential functions. The fast components (~5–7 μs) were derived from the WO_3–V_O complex defects according to the decay times since the PMT for the NIR range also had a sensitivity down to ~500 nm. The slow components had decay times of ~160–220 μs. They are typical values as Nd^{3+} 4f–4f transitions reported in some materials doped with Nd [44,45]. The scintillation decay times of the emissions at 1060 and 1300 nm could not be measured in the study owing to the limitation of sensitivity of the PMT. However, the decay times of the transitions at 1060 and 1300 nm can be respectively estimated to ~370 and ~580 μs according to the relationship between decay times and wavelength of scintillation ($\tau \sim \lambda^{2.2}$, where τ means the scintillation decay time and λ means emission wavelength) [46]. In the assumed applications, signal accumulation time is from several seconds to minutes, and the decay times observed here are acceptable enough for these applications.

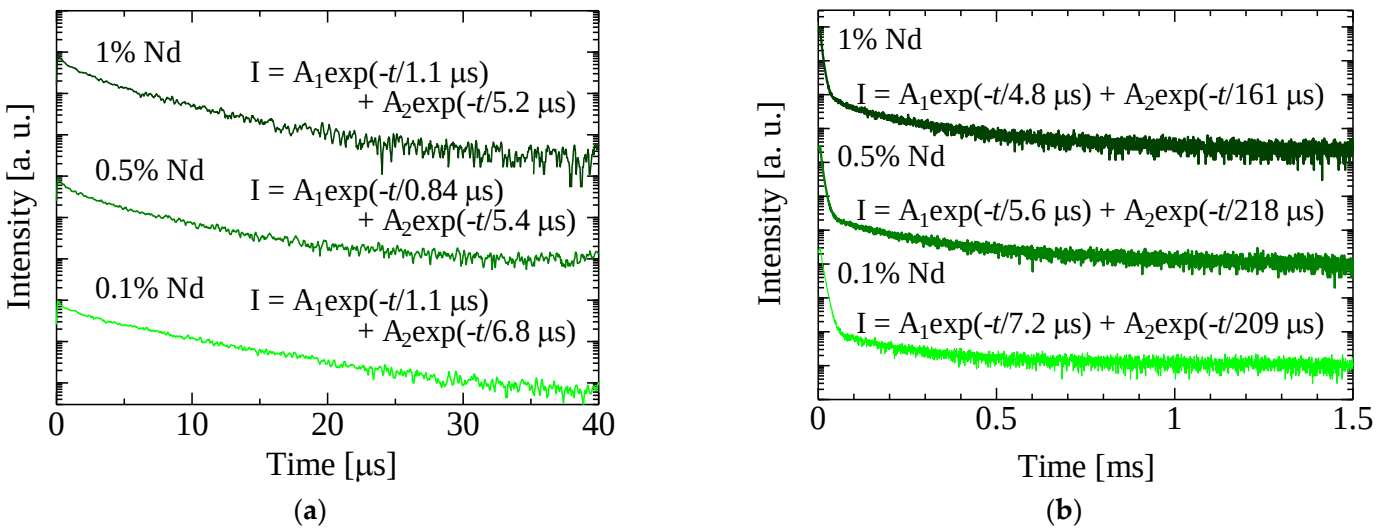

Figure 7. X-ray-induced scintillation decay curves of Nd-doped $CaWO_4$ monitored (**a**) UV–visible ranges and (**b**) visible–NIR ranges.

Afterglow curves after 2 ms X-ray exposure of the crystals are exhibited in Figure 8. Afterglow demonstrates a relaxation process of electrons trapped at ~25meV from the bottom of the conduction band by thermal stimulation. The afterglow levels (A) were calculated as follows: $A = (I_{20} - I_{bg})/(I_{max} - I_{bg})$. Here, I_{20}, I_{max}, and I_{bg} were intensity at 20 ms after irradiation of X-ray, intensity during irradiation of X-ray, and intensity before irradiation of X-ray. The As of 0.1, 0.5, and 1% Nd-doped crystals were respectively estimated to be 1330, 1080, and 390 ppm. The As were much higher than that of $CdWO_4$ (~10 ppm [31]). However, the value of the 1% Nd-doped crystal was comparable to that of Tl-doped CsI (~300 ppm [47]), one of the representative commercial scintillators for X-ray detection.

Relationships between the X-ray irradiated dose rate and the signal intensity in NIR ranges were investigated. In Figure 9, the vertical and horizontal axes present the averaged currents during X-ray exposure subtracted by averaged currents before X-ray exposure (background level) and X-ray exposure dose rate, respectively. The 0.5% Nd-doped crystal showed a response with retaining the linearity from 0.06 to 60 Gy/h with retaining the linearity whereas that of 0.1 and 1% Nd-doped crystals were 0.3–60 Gy/h. In the conventional model [48], the scintillation light yields (LYs) depend on the QY; thus, the 0.5%Nd-doped crystal is considered to show the highest LY among the present crystals, although the quantitative evaluation of the LYs in NIR ranges could not be done owing to the decay times with several hundred μs of Nd^{3+}. The difference in LY would result in the difference in dynamic ranges among the crystals. In the past study, some of the Nd-doped materials were evaluated as NIR-scintillators by using the same detector form: SrY_2O_4

(0.06–60 Gy/h [49]), $Bi_4Ge_3O_{12}$ (0.01–60 Gy/h [38]), and $LuVO_4$ (0.006–60 Gy/h [50]). The present results were inferior to the lowest dose rate retaining the linearity (0.006 Gy/h) reported in the past studies; however, they were comparable with the second-best dose rate (~0.01 Gy/h). When compared with other red or NIR-scintillators combined with Si-based detectors, the detection limit in the present result was superior to that of Cs_2HfI_6 (2 Gy/h) and commercial Pr-doped Gd_2O_2S (GOS) (0.8 Gy/h) [20,51]. Additionally, we compared the present results with previous ones of visible-scintillation detectors such as $CdWO_4$ combined with a PMT and Tb-doped GOS, which coated to a polymethyl methacrylate-based fiber combined with a Si-CCD. The lowest detectable dose rates of $CdWO_4$ and Tb-doped GOS-based detectors were ~0.05 and ~60 Gy/h [52,53], and the present results surpassed these widely used commercial scintillators. The dose rate response of the $CdWO_4$ and Tb-doped GOS could not be measured in this research since their emission wavelength (~500 nm) was out of the wavelength sensitivity of the InGaAs-PD (>900 nm).

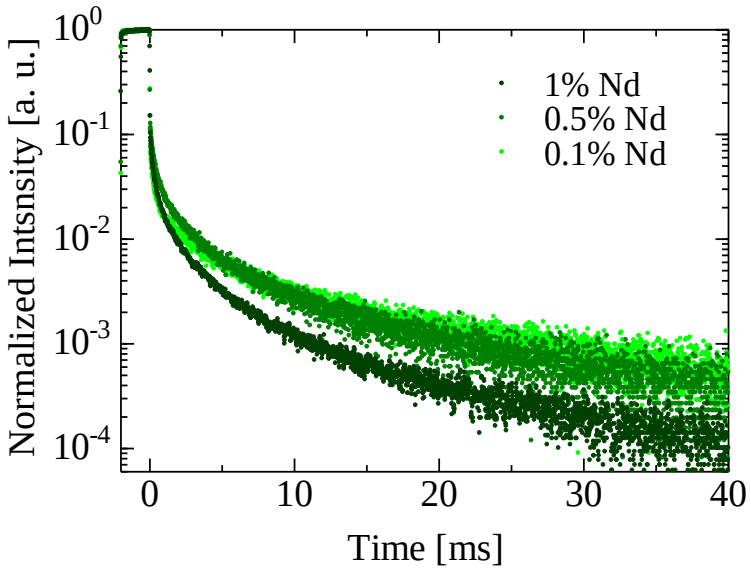

Figure 8. Afterglow curves of Nd-doped $CaWO_4$.

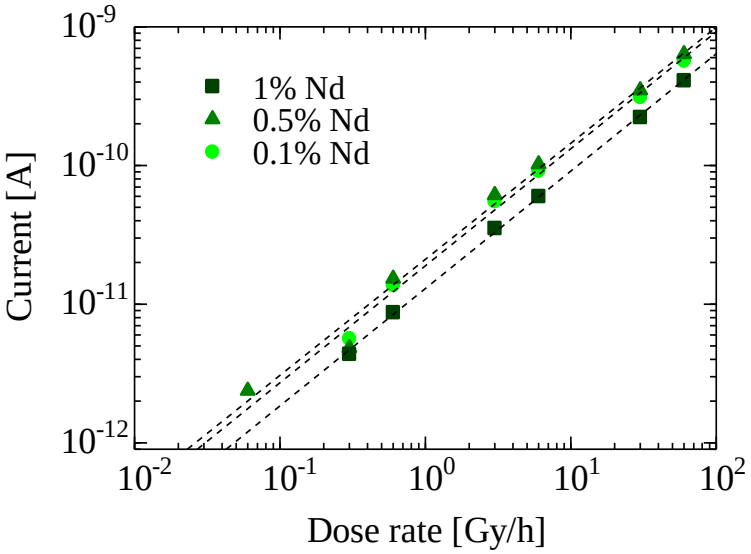

Figure 9. Relationships between the X-ray exposure dose rate and the intensity in the NIR ranges of the crystals.

4. Conclusions

$CaWO_4$ single crystals doped with Nd (0.1, 0.5, and 1%) were grown by the FZ method. The optical and scintillation characteristics were investigated. Typical luminescence and decay times due to the Nd^{3+} transitions were confirmed when monitored at NIR ranges. To confirm the performance of NIR scintillation detectors, X-ray irradiated dose rate response properties were evaluated by using the crystals and an InGaAs-PD. The 0.5% Nd-doped crystal indicated the widest dynamic range (0.06–60 Gy/h) in all the present crystals. The result was comparable to the measurable ranges of other Nd-doped phosphors combined with an InGaAs-PD, such as Nd-doped SrY_2O_4 and Nd-doped $Bi_4Ge_3O_{12}$, and it was superior to that of other scintillators emitting red light combined with Si-based detectors: Cs_2HfI_6 and commercial Pr-doped Gd_2O_2S. From the study, Nd-doped $CaWO_4$ crystals were suggested to have the potential as NIR-scintillators used in high-dose field monitoring.

Author Contributions: Conceptualization, K.O.; methodology, K.O. and H.F.; validation, H.F., D.N., T.K., N.K. and T.Y.; formal analysis, K.O. and D.N.; investigation, K.O., D.N. and T.Y.; resources, T.Y.; data curation, K.O.; writing—original draft preparation, K.O.; writing—review and editing, K.O. and T.Y.; visualization, K.O.; supervision, T.Y.; project administration, T.Y.; funding acquisition, D.N., T.K., N.K. and T.Y. All authors have read and agreed to the published version of the manuscript.

Funding: This work was supported by Grant-in-Aid for Scientific Research A (22H00309), Scientific Research B (21H03733, 21H03736, and 22H03872), and Exploratory Research (22K18997) from Japan Society for the Promotion of Science. JST A-STEP, Foundation from Cooperative Research Project of Research Center for Biomedical Engineering, Nippon Sheet Glass Foundation, Terumo Life Science Foundation, Iwatani Naoji Foundation, and Konica Minolta Science and Technology Foundation are also acknowledged.

Institutional Review Board Statement: Not applicable.

Informed Consent Statement: Not applicable.

Data Availability Statement: Not applicable.

Conflicts of Interest: The authors declare no conflict of interest.

References

1. Weber, M.J. Inorganic scintillators: Today and tomorrow. *J. Lumin.* **2002**, *100*, 35–45. [CrossRef]
2. van Eijk, C.W.E. Inorganic scintillators in medical imaging detectors. *Nucl. Instrum. Methods Phys. Res. A Accel. Spectrom. Detect. Assoc. Equip.* **2003**, *509*, 17–25. [CrossRef]
3. Ryzhikov, V.D.; Opolonin, A.D.; Pashko, P.V.; Svishch, V.M.; Volkov, V.G.; Lysetskaya, E.K.; Kozin, D.N.; Smith, C. Instruments and detectors on the base of scintillator crystals ZnSe(Te), CWO, CsI(Tl) for systems of security and customs inspection systems. *Nucl. Instrum. Methods Phys. Res. A Accel. Spectrom. Detect. Assoc. Equip.* **2005**, *537*, 424–430. [CrossRef]
4. de Faoite, D.; Hanlon, L.; Roberts, O.; Ulyanov, A.; McBreen, S.; Tobin, I.; Stanton, K.T. Development of glass-ceramic scintillators for gamma-ray astronomy. *J. Phys. Conf. Ser.* **2015**, *620*, 012002. [CrossRef]
5. Lecoq, P.; Korzhik, M. Scintillator developments for high energy physics and medical imaging. *IEEE Trans. Nucl. Sci.* **2000**, *47*, 1311–1314. [CrossRef]
6. Melcher, C.L.; Schweitzer, J.S.; Manente, R.A.; Peterson, C.A. Applications of single crystals in oil well logging. *J. Cryst. Growth* **1991**, *109*, 37–42. [CrossRef]
7. Nagarkar, V.V.; Gupta, T.K.; Miller, S.R.; Klugerman, Y.; Squillante, M.R.; Entine, G. Structured CsI(Tl) scintillators for X-ray imaging applications. *IEEE Trans. Nucl. Sci.* **1998**, *45*, 492–496. [CrossRef]
8. Melcher, C.L.; Schweitzer, J.S. A promising new scintillator: Cerium-doped lutetium oxyorthosilicate. *Nucl. Instrum. Methods Phys. Res. A Accel. Spectrom. Detect. Assoc. Equip.* **1992**, *314*, 212–214. [CrossRef]
9. Takagi, K.; Fukazawa, T. Cerium-activated Gd_2SiO_5 single crystal scintillator. *Appl. Phys. Lett.* **1983**, *42*, 43–45. [CrossRef]
10. Quarati, F.G.A.; Owens, A.; Dorenbos, P.; de Haas, J.T.M.; Benzoni, G.; Blasi, N.; Boiano, C.; Brambilla, S.; Camera, F.; Alba, R.; et al. High energy gamma-ray spectroscopy with $LaBr_3$ scintillation detectors. *Nucl. Instrum. Methods Phys. Res. A Accel. Spectrom. Detect. Assoc. Equip.* **2011**, *629*, 157–169. [CrossRef]
11. Farrell, R.; Olschner, F.; Shah, K.; Squillante, M.R. Advances in semiconductor photodetectors for scintillators. *Nucl. Instrum. Methods Phys. Res. A Accel. Spectrom. Detect. Assoc. Equip.* **1997**, *387*, 194–198. [CrossRef]
12. Sakai, E. Recent Measurements on Scintillator-Photodetector Systems. *IEEE Trans. Nucl. Sci.* **1987**, *34*, 418–422. [CrossRef]
13. Theocharous, E. Absolute linearity measurements on a PbS detector in the infrared. *Appl. Opt.* **2006**, *45*, 2381–2386. [CrossRef] [PubMed]

14. Wei, C.Y.; Wang, K.L.; Taft, E.A.; Swab, J.M.; Gibbons, M.D.; Davern, W.E.; Brown, D.M. Technology development for InSb infrared imagers. *IEEE Trans. Electron Devices* **1980**, *27*, 170–175. [CrossRef]
15. Maruyama, T. Development of a near-infrared photon-counting system using an InGaAs avalanche photodiode. *Opt. Eng.* **2002**, *41*, 395. [CrossRef]
16. Nakauchi, D.; Fujimoto, Y.; Kato, T.; Kawaguchi, N.; Yanagida, T. Properties of Sm-Doped $SrCl_2$ Crystalline Scintillators. *Crystals* **2022**, *12*, 517. [CrossRef]
17. Duan, Y.; Liu, B. Recent Advances of Optical Imaging in the Second Near-Infrared Window. *Adv. Mater.* **2018**, *30*, 1802394. [CrossRef]
18. Nakauchi, D.; Fujimoto, Y.; Kato, T.; Kawaguchi, N.; Yanagida, T. X- and γ-ray response of Sm-doped $SrBr_2$ crystalline scintillators emitting red-NIR photons. *Jpn. J. Appl. Phys.* **2021**, *60*, 092002. [CrossRef]
19. Kaptanoglu, T.; Luo, M.; Klein, J. Cherenkov and scintillation light separation using wavelength in LAB based liquid scintillator. *J. Instrum.* **2019**, *14*, T05001. [CrossRef]
20. Takada, E.; Kimura, A.; Hosono, Y.; Takahashi, H.; Nakazawa, M. Radiation Distribution Sensor with Optical Fibers for High Radiation Fields. *J. Nucl. Sci. Technol.* **1999**, *36*, 641–645. [CrossRef]
21. Irshad Ahamed, M.; Sathish Kumar, K. Studies on Cu_2SnS_3 quantum dots for O-band wavelength detection. *Mater. Sci.* **2019**, *37*, 225–229. [CrossRef]
22. Rodnyi, P.A. *Physical Processes in Inorganic Scintillators*; New York CRC Press: New York, NY, USA, 1997.
23. Baccaro, S.; Bohacek, P.; Cecilia, A.; Laguta, V.; Montecchi, M.; Mihokova, E.; Nikl, M. Effect of La Doping on Calcium Tungstate ($CaWO_4$) Crystals Radiation Hardness. *Phys. Status Solidi* **2000**, *178*, 799–804. [CrossRef]
24. Okazaki, K.; Fukushima, H.; Nakauchi, D.; Okada, G.; Onoda, D.; Kato, T.; Kawaguchi, N.; Yanagida, T. Luminescence and dose-rate response properties of Pr-doped $Bi_4Ge_3O_{12}$ scintillators. *Radiat. Meas.* **2022**, *154*, 106773. [CrossRef]
25. Meral, G.; Tasar, F.; Kocagöz, S.; Sener, C. Factors affecting the antibacterial effects of Nd:YAG laser in vivo. *Lasers Surg. Med.* **2003**, *32*, 197–202. [CrossRef] [PubMed]
26. Yanagida, T.; Fujimoto, Y.; Ishizu, S.; Fukuda, K. Optical and scintillation properties of Nd differently doped $YLiF_4$ from VUV to NIR wavelengths. *Opt. Mater.* **2015**, *41*, 36–40. [CrossRef]
27. Kantuptim, P.; Akatsuka, M.; Nakauchi, D.; Kato, T.; Kawaguchi, N.; Yanagida, T. Optical and scintillation properties of Nd-doped $Lu_2Si_2O_7$ single crystals. *J. Alloys Compd.* **2021**, *860*, 158538. [CrossRef]
28. Fujimoto, Y.; Yanagida, T.; Kojima, T.; Koshimizu, M.; Hironori, T.; Keisuke, A. Optical and Near-Infrared Scintillation Properties of Nd^{3+}-Doped YVO_4 Crystals. *Sens. Mater.* **2016**, *28*, 857–861. [CrossRef]
29. Akatsuka, M.; Kimura, H.; Onoda, D.; Shiratori, D.; Nakauchi, D.; Kato, T.; Kawaguchi, N.; Yanagida, T. X-ray-induced Luminescence Properties of Nd-doped $GdVO_4$. *Sens. Mater.* **2021**, *33*, 2243–2250. [CrossRef]
30. Yanagida, T.; Kamada, K.; Fujimoto, Y.; Yagi, H.; Yanagitani, T. Comparative study of ceramic and single crystal Ce:GAGG scintillator. *Opt. Mater.* **2013**, *35*, 2480–2485. [CrossRef]
31. Yanagida, T.; Fujimoto, Y.; Ito, T.; Uchiyama, K.; Mori, K. Development of X-ray-induced afterglow characterization system. *Appl. Phys. Express* **2014**, *7*, 062401. [CrossRef]
32. Yaba, T.; Wangkhem, R.; Singh, N.S. Enhanced red emission from Bi^{3+} sensitized $CaWO_4$:Eu^{3+} as red component for near UV/blue LED pumped white light emission. *J. Alloys Compd.* **2020**, *843*, 156022. [CrossRef]
33. Kang, F.; Hu, Y.; Chen, L.; Wang, X.; Mu, Z.; Wu, H.; Ju, G. Eu^{3+} Doped $CaWO_4$—A Potential Red Long Afterglow Phosphor. *Appl. Phys. B* **2012**, *107*, 833–837. [CrossRef]
34. Suneetha, P.; Rajesh, C.; Ramana, M.V. Nd-doped $CaWO_4$ nanocrystals—Synthesis and characterization. *Mater. Res. Express* **2017**, *4*, 085020. [CrossRef]
35. Das, D.; Gupta, S.K.; Datrik, C.S.; Nandi, P.; Sudarshan, K. Role of alkali charge compensation in the luminescence of $CaWO_4$:Nd^{3+} and $SrWO_4$:Nd^{3+} Scheelites. *New J. Chem.* **2020**, *44*, 7300–7309. [CrossRef]
36. Kang, F.; Peng, M. A new study on the energy transfer in the color-tunable phosphor $CaWO_4$:Bi. *Dalton Trans.* **2014**, *43*, 277–284. [CrossRef] [PubMed]
37. Wei, Y.; Tu, C.; Wang, H.; Yang, F.; Jia, G.; You, Z.; Lu, X.; Li, J.; Zhu, Z.; Wang, Y. Optical properties of Nd^{3+}:NaLa $(WO_4)_2$ single crystal. *Opt. Mater.* **2007**, *29*, 1653–1657. [CrossRef]
38. Okazaki, K.; Onoda, D.; Fukushima, H.; Nakauchi, D.; Kato, T.; Kawaguchi, N.; Yanagida, T. Characterization of scintillation properties of Nd-doped $Bi_4Ge_3O_{12}$ single crystals with near-infrared luminescence. *J. Mater. Sci. Mater. Electron.* **2021**, *32*, 21677–21684. [CrossRef]
39. Kraus, H.; Mikhailik, V.B.; Ramachers, Y.; Day, D.; Hutton, K.B.; Telfer, J. Feasibility study of a $ZnWO_4$ scintillator for exploiting materials signature in cryogenic WIMP dark matter searches. *Phys. Lett. Sect. B Nucl. Elem. Part. High-Energy Phys.* **2005**, *610*, 37–44. [CrossRef]
40. Nakauchi, D.; Okada, G.; Koshimizu, M.; Yanagida, T. Optical and scintillation properties of Nd-doped $SrAl_2O_4$ crystals. *J. Rare Earths* **2016**, *34*, 757–762. [CrossRef]
41. Akatsuka, M.; Nakauchi, D.; Kato, T.; Kawaguchi, N.; Yanagida, T. Characterization of Nd: $LaVO_4$ single-crystal scintillator emitting near-infrared photons. *Jpn. J. Appl. Phys.* **2022**, *61*, SB1025. [CrossRef]
42. Okada, G.; Kawaguchi, N.; Yanagida, T. Development of NIR-Emitting Scintillators Based on Rare-Earth-Doped Garnet Crystals—Part 1. *Sens. Mater.* **2017**, *29*, 1407–1415. [CrossRef]

43. Zorenko, Y.; Pashkovsky, M.; Voloshinovskii, A.; Kuklinski, B.; Grinberg, M. The luminescence of $CaWO_4$: Bi single crystals. *J. Lumin.* **2006**, *116*, 43–51. [CrossRef]
44. Yanagida, T.; Akatsuka, M.; Okada, G.; Kawaguchi, N. Optical and scintillation properties of Nd-doped $YAlO_3$ crystals. *Opt. Mater.* **2019**, *90*, 14–19. [CrossRef]
45. Akatsuka, M.; Nakauchi, D.; Kato, T.; Kawaguchi, N.; Yanagida, T. Scintillation properties of Nd-doped $MSiO_3$ (M = Ca, Sr, Ba) single crystals. *Radiat. Meas.* **2020**, *133*, 106298. [CrossRef]
46. Yanagida, T. Inorganic scintillating materials and scintillation detectors. *Proc. Jpn. Acad. Ser. B* **2018**, *94*, 75–97. [CrossRef] [PubMed]
47. Nakauchi, D.; Kato, T.; Kawaguchi, N.; Yanagida, T. Characterization of Eu-doped Ba_2SiO_4, a high light yield scintillator. *Appl. Phys. Express* **2020**, *13*, 122001. [CrossRef]
48. Robbins, D.J. On Predicting the Maximum Efficiency of Phosphor Systems Excited by Ionizing Radiation. *J. Electrochem. Soc.* **1980**, *127*, 2694–2702. [CrossRef]
49. Fukushima, H.; Akatsuka, M.; Kimura, H.; Onoda, D.; Shiratori, D.; Nakauchi, D.; Kato, T.; Kawaguchi, N.; Yanagida, T. Optical and Scintillation Properties of Nd-doped Strontium Yttrate Single Crystals. *Sens. Mater.* **2021**, *33*, 2235–2241. [CrossRef]
50. Akatsuka, M.; Nakauchi, D.; Kato, T.; Noriaki, K.; Takayuki, Y. Scintillation Properties of Nd-doped $LuVO_4$ Single Crystals. *Sens. Mater.* **2022**, *34*, 619–627. [CrossRef]
51. Kodama, S.; Kurosawa, S.; Ohno, M.; Morishita, Y.; Usami, H.; Hayashi, M.; Sasano, M.; Azuma, T.; Tanaka, H.; Kochurikhin, V.; et al. Fiber-read radiation monitoring system using an optical fiber and red-emitting scintillator for ultra-high-dose conditions. *Appl. Phys. Express* **2020**, *13*, 047002. [CrossRef]
52. Michail, C.; Koukou, V.; Martini, N.; Saatsakis, G.; Kalyvas, N.; Bakas, A.; Kandarakis, I.; Fountos, G.; Panayiotakis, G.; Valais, I. Luminescence Efficiency of Cadmium Tungstate ($CdWO_4$) Single Crystal for Medical Imaging Applications. *Crystals* **2020**, *10*, 429. [CrossRef]
53. Lewis, E.; O'Keeffe, S.; Grattan, M.; Hounsell, A.; McCarthy, D.; Woulfe, P.; Cronin, J.; Mihai, L.; Sporea, D.; Santhanam, A.; et al. Terbium-doped gadolinium oxysulfide (Gd_2O_2S:Tb) scintillation-based polymer optical fibre sensor for real time monitoring of radiation dose in oncology. *Opt. Sens. Detect. III* **2014**, *9141*, 914113. [CrossRef]